Electronic Supporting Information (ESI)

Fundamental Interplay between phase-transition kinetics and thermodynamics of manganese-based sodium layered oxides during cationic and anionic redox

Hyungjun Kim[b‡], Jaewoon Lee [a‡], Myungkyu Kim[b], Sojung Koo[a], Maenghyo Cho[b*], Duho Kim[a*]

[a]Department of Mechanical Engineering, Kyung Hee University, 1732, Deogyeong-daero, Giheung-gu, Yongin-si, Gyeonggi-do, 17104, Republic of Korea
[b]Department of Mechanical and Aerospace Engineering, Seoul National University, 1 Gwanak-ro, Gwanak-gu, Seoul 08826, Republic of Korea
[‡]There authors contributed equally

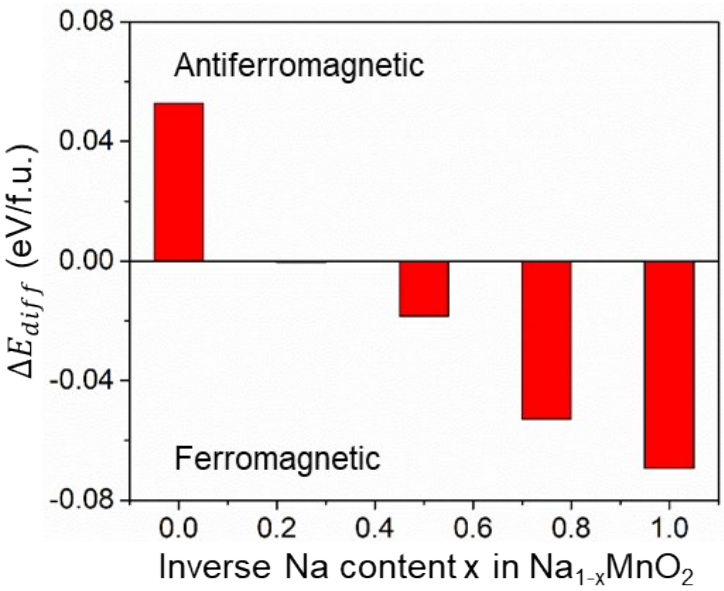

Figure S1. Energy differences between the antiferromagnetic and ferromagnetic states of the ground states ($x = 0.0, 0.25, 0.5, 0.75, and\ 1.0$) for $Na_{1-x}MnO_2$.

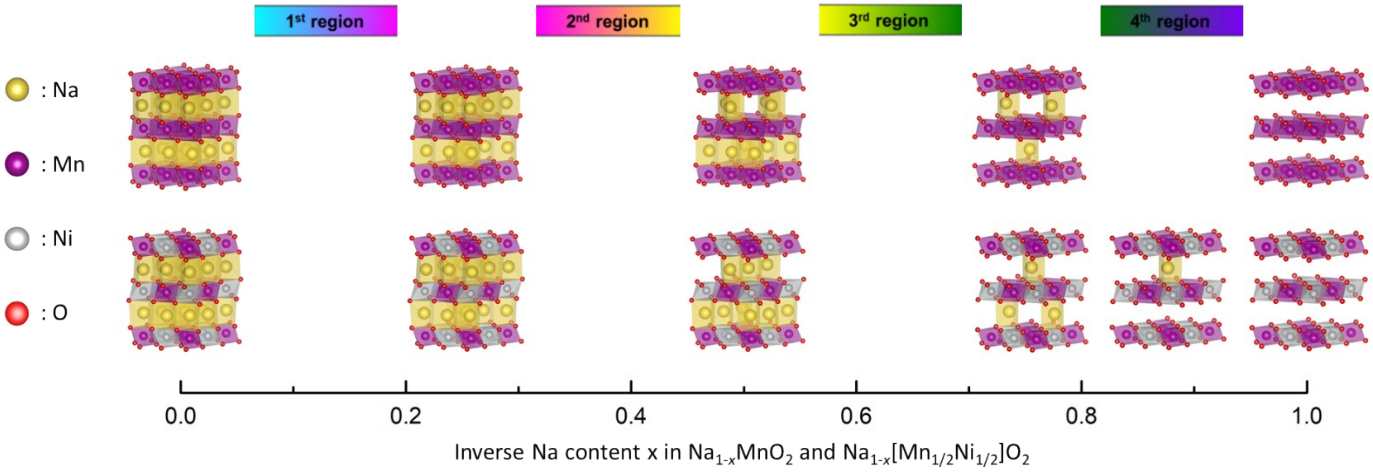

Figure S2. The ground states configurations of $Na_{1-x}MnO_2$ (upper) and $Na_{1-x}[Mn_{1/2}Ni_{1/2}]O_2$ (lower) following the desodiation process.

Inverse Na content x in $Na_{1-x}MnO_2$	Unit cell volume (Å^3)	a parameter (Å)	b parameter (Å)	c parameter (Å)
0.0	358.913	5.973	5.973	11.255
0.125	-	-	-	-
0.25	343.135	6.057	5.707	11.254
0.375	-	-	-	-
0.5	349.178	6.026	5.718	11.460
0.625	-	-	-	-
0.75	333.583	5.720	5.725	11.771
0.875	-	-	-	-
1.0	305.120	5.767	5.767	10.593

Inverse Na content x in $Na_{1-x}[Mn_{1/2}Ni_{1/2}]O_2$	Unit cell volume (Å^3)	a parameter (Å)	b parameter (Å)	c parameter (Å)
0.0	340.585	5.971	5.971	11.081
0.125	-	-	-	-
0.25	335.817	5.921	5.914	11.184
0.375	-	-	-	-
0.5	330.737	5.905	5.822	11.318
0.625	-	-	-	-
0.75	333.952	5.736	5.676	11.726
0.875	316.121	5.739	5.739	11.042
1.0	289.194	5.719	5.719	10.185

Table S1. Volume and lattice parameters of the atomic structure for $Na_{1-x}MnO_2$ (upper table) and $Na_{1-x}[Mn_{1/2}Ni_{1/2}]O_2$ (lower table) calculated by first-principles calculations under 550 eV plane wave cutoff energy.

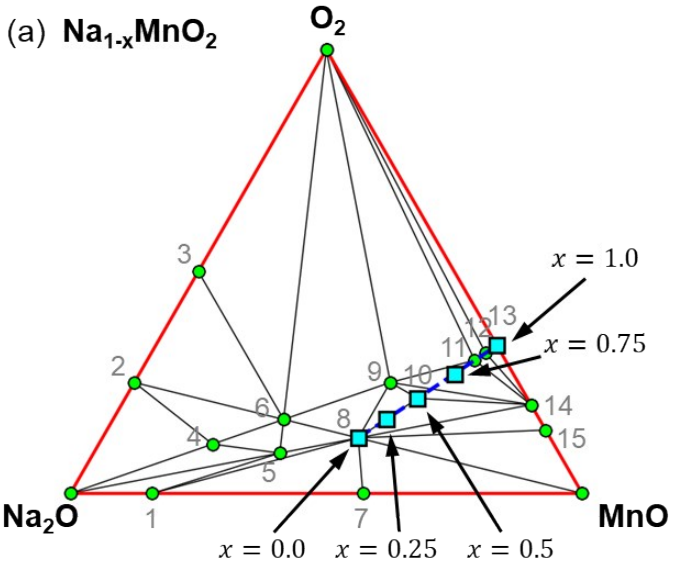

#	Formula	mp-ID
1	$Na_{14}Mn_2O_9$	mp-27569
2	Na_2O_2	mp-2340
3	NaO_2	mp-1901
4	Na_4MnO_4	mp-849304
5	$Na_4Mn_2O_5$	mp-18869
6	Na_2MnO_3	mp-761229
7	$Na_2Mn_2O_3$	mp-558376
8	$NaMnO_2$	mp-18957
9	$Na_2Mn_3O_7$	mp-19080
10	$NaMn_2O_4$	mp-542710
11	$NaMn_8O_{16}$	mp-1003638
12	$NaMn_{16}O_{32}$	mp-1003635
13	MnO_2	mp-19395
14	Mn_2O_3	mp-1172875
15	Mn_3O_4	mp-18759

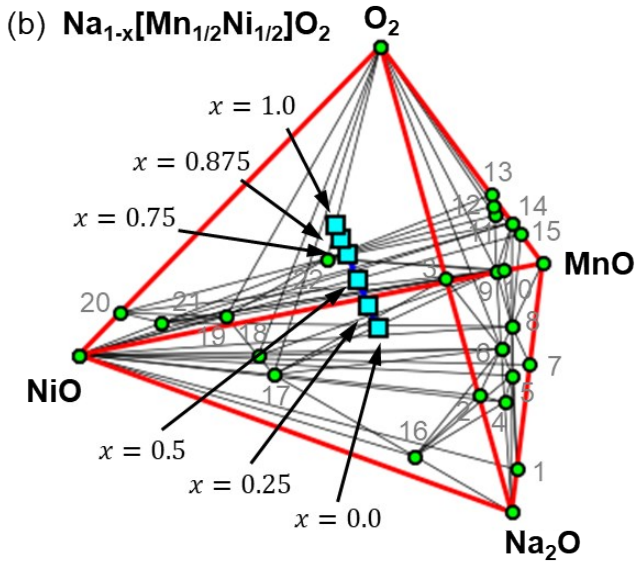

#	Formula	mp-ID
16	Na_5NiO_4	mp-21996
17	$NaNiO_2$	mp-19149
18	$Na_4(NiO_2)_5$	mp-753301
19	$Na_4(NiO_2)_9$	mp-764295
20	Ni_3O_4	mp-656887
21	$Mn(Ni_3O_4)_2$	mp-19442
22	$MnNiO_3$	mp-19331

Figure S3. Compound, (a) Na_2O–MnO–O_2 and (b) Na_2O–MnO–NiO–O_2, phase diagram. Green dots represent the stable phases, and red and black lines express equilibrium tie lines, while cyan squares display $Na_{1-x}MnO_2$ (at $x = 0.0, 0.25, 0.5, 0.75,$ and 1.0) and $Na_{1-x}[Mn_{1/2}Ni_{1/2}]O_2$ (at $x = 0.0, 0.25, 0.5, 0.75, 0.875,$ and 1.0). The stable phases (green dots) are tabulated on the right tables with their Materials Project ID.

(a) $Na_{1-x}MnO_2$

x	Decomposition products	Decomposition energy (eV/atom)
0.0	$NaMnO_2$	0.105
0.25	$NaMnO_2$, $NaMn_2O_4$	0.054
0.50	$NaMn_2O_4$	0.023
0.75	$NaMn_8O_{16}$, $Na_2Mn_3O_7$, Mn_2O_3	0.019
1.0	MnO_2	0.015

(b) $Na_{1-x}[Mn_{1/2}Ni_{1/2}]O_2$

x	Decomposition products	Decomposition energy (eV/atom)
0.0	Na_2MnO_3, NiO	0.028
0.25	$Na_2Mn_3O_7$, Na_2MnO_3, NaO_2, NiO	0.008
0.50	$Na_2Mn_3O_7$, NaO_2, NiO	0.022
0.75	$MnNiO_3$, NaO_2	0.067
0.875	$MnNiO_3$, NaO_2, O_2	0.088
1.0	$MnNiO_3$, O_2	0.094

Table S2. Decomposition products and corresponding reaction energy for each ground state for (a) $Na_{1-x}MnO_2$ (at $x = 0.0, 0.25, 0.5, 0.75,$ and 1.0) and (b) $Na_{1-x}[Mn_{1/2}Ni_{1/2}]O_2$ (at $x = 0.0, 0.25, 0.5, 0.75, 0.875,$ and 1.0).

Although each stable ground state during desodiation appears to decompose at 0 K equilibrium phase diagram, $Na_{1-x}MnO_2$ and $Na_{1-x}[Mn_{1/2}Ni_{1/2}]O_2$ are able to be synthesized with elaborate experimental methods.[S1-S3] Additionally, considering the comparatively low reaction energy for decomposition (~ 100 meV/atom) of each ground state in $Na_{1-x}MnO_2$ and $Na_{1-x}[Mn_{1/2}Ni_{1/2}]O_2$ and kinetic difficulty for Mn and Ni to rearrange and form decomposition products, $Na_{1-x}MnO_2$ and $Na_{1-x}[Mn_{1/2}Ni_{1/2}]O_2$ are thermodynamically stable.

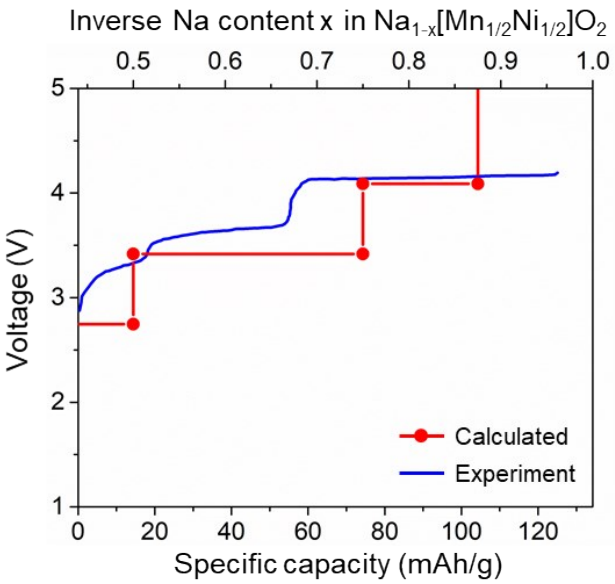

Figure S4. Calculated desodiation potentials of $Na[Mn_{1/2}Ni_{1/2}]O_2$ with the experimentally measured charge profile reproduced from Ref. S4,S5.

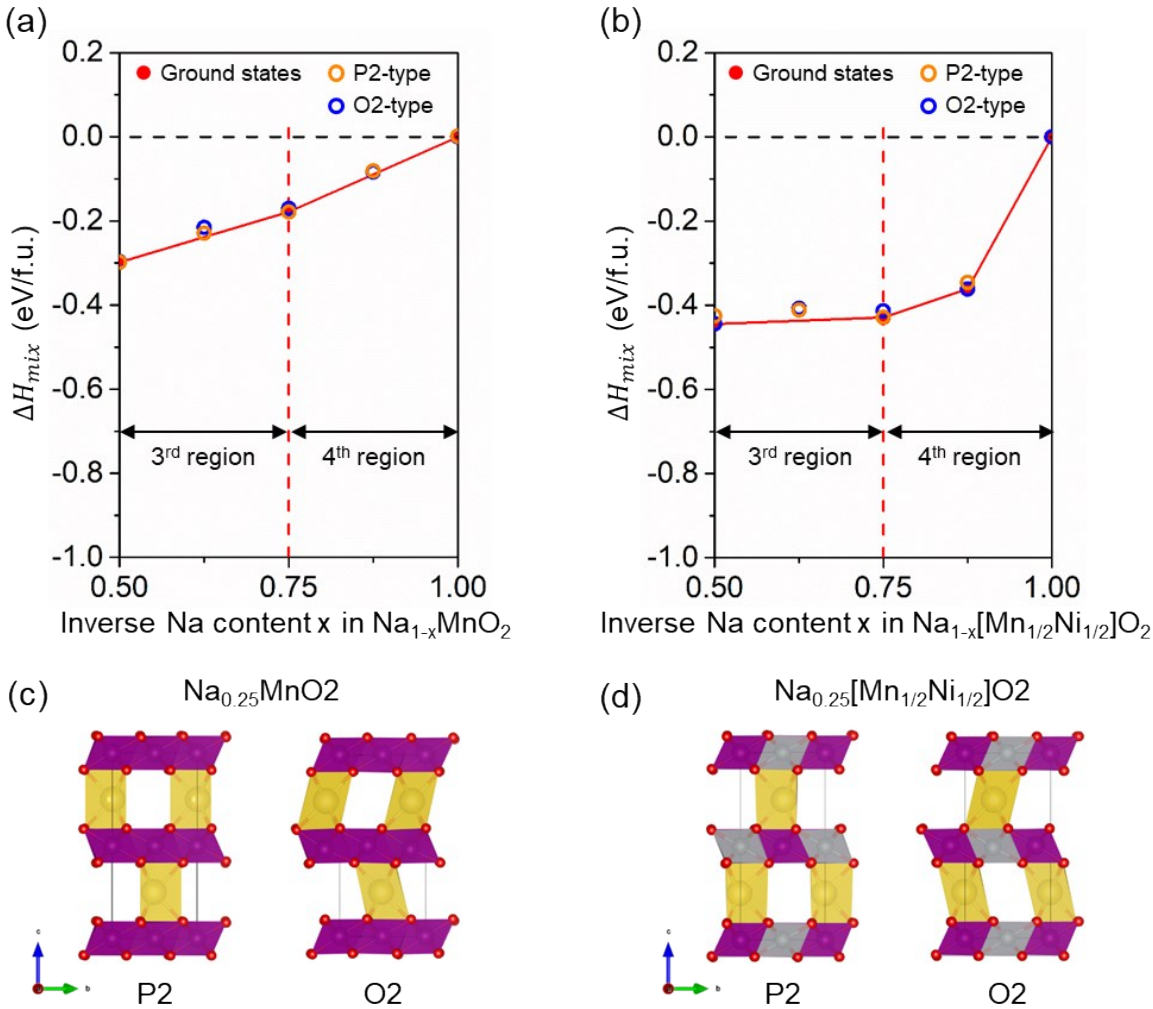

Figure S5. Formation energies of mixing enthalpy considering both Na/□ orderings and interlayer stacking changes (P2- or O2-stacking) as a function of the inverse Na content (x) for (a) $Na_{1-x}MnO_2$ and (b) $Na_{1-x}[Mn_{1/2}Ni_{1/2}]O_2$ oxides in the anion-redox-related regions (3rd $0.5 \leq x \leq 0.75$, and 4th $0.75 \leq x \leq 1.0$). Atomic structure of P2- or O2-stacking for (c) $Na_{1-x}MnO_2$ and (d) $Na_{1-x}[Mn_{1/2}Ni_{1/2}]O_2$ at $x = 0.75$.

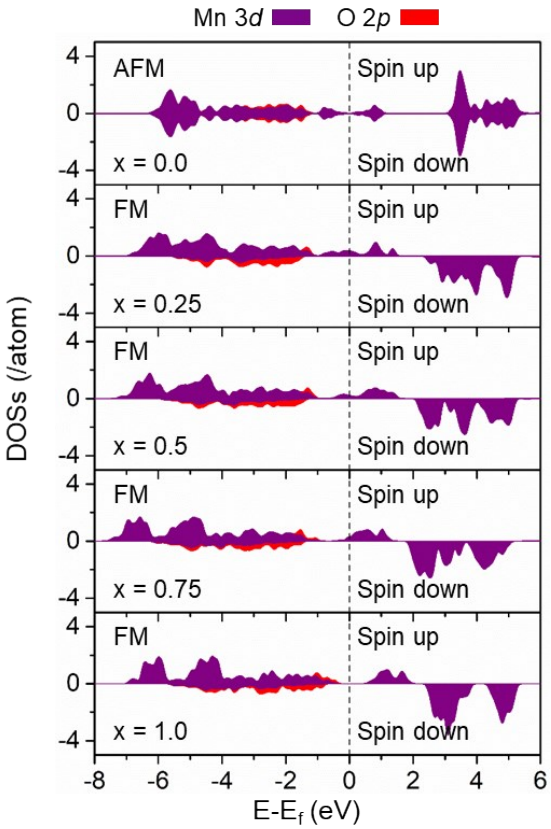

Figure S6. Combined profiles of partial density of states (PDOSs) of Mn 3*d*-electron and O 2*p*-electron at $x = 0.0, 0.25, 0.5, 0.75, and\ 1.0$ in $Na_{1-x}MnO_2$.

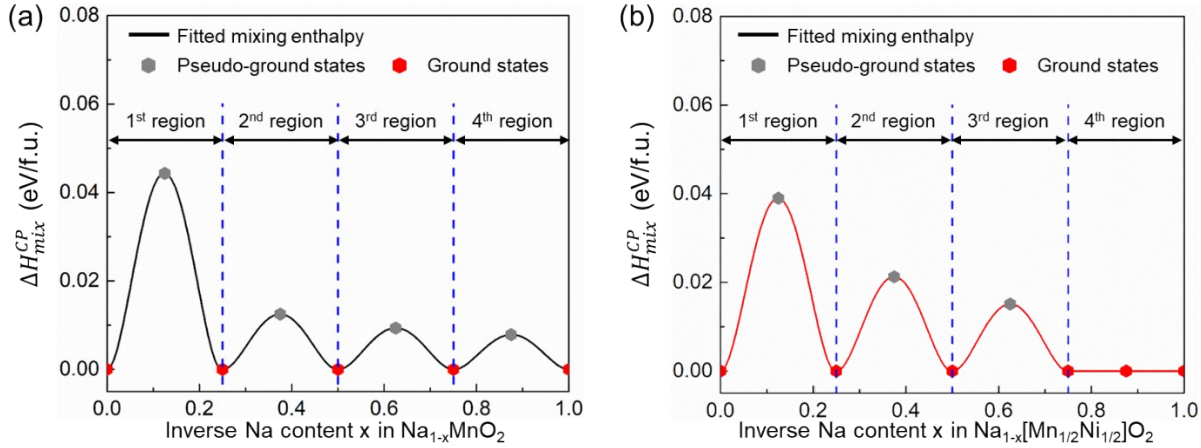

Figure S7. Combined-phase mixing enthalpy fitted from the ground/pseudo-ground states from first-priniciple formation energies of mixing enthalpy (a) in $NaMnO_2$ and (b) in $Na[Mn_{1/2}Ni_{1/2}]O_2$, from Figure 1a-b using the quadratic double-well function.

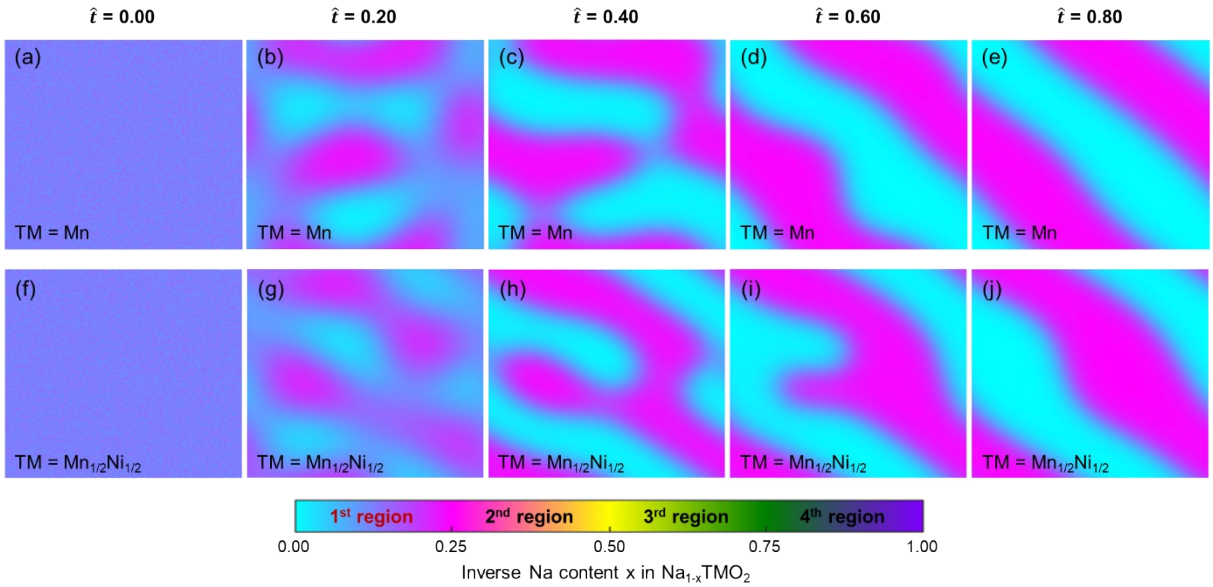

Figure S8. Contours of phase separation kinetics of (a-e) $NaMnO_2$ and (f-j) $Na[Mn_{1/2}Ni_{1/2}]O_2$ in 1st region at different dimensionless times $\hat{t}$ ($\hat{t}$ = 0.00, 0.20, 0.40, 0.60, and 0.80).

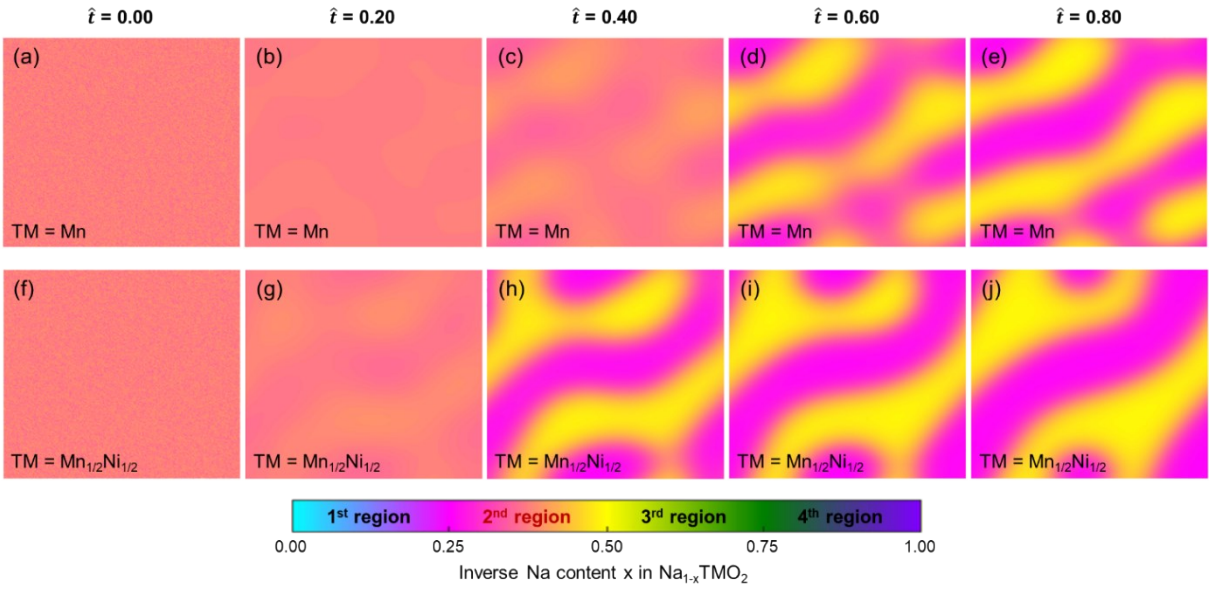

Figure S9. Contours of phase separation kinetics of (a-e) $NaMnO_2$ and (f-j) $Na[Mn_{1/2}Ni_{1/2}]O_2$ in the 2nd region at different dimensionless times $\hat{t}$ ($\hat{t}$ = 0.00, 0.20, 0.40, 0.60, and 0.80).

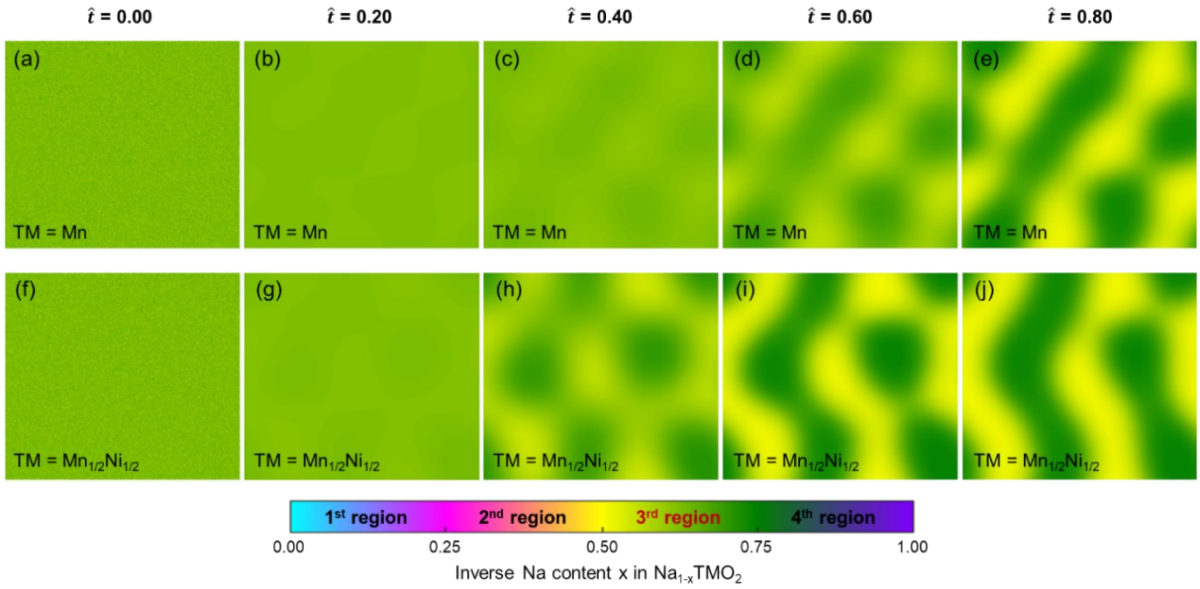

Figure S10. Contours of phase separation kinetics of (a-e) $NaMnO_2$ and (f-j) $Na[Mn_{1/2}Ni_{1/2}]O_2$ in the 3rd region at different dimensionless times $\hat{t}$ ($\hat{t}$ = 0.00, 0.20, 0.40, 0.60, and 0.80).

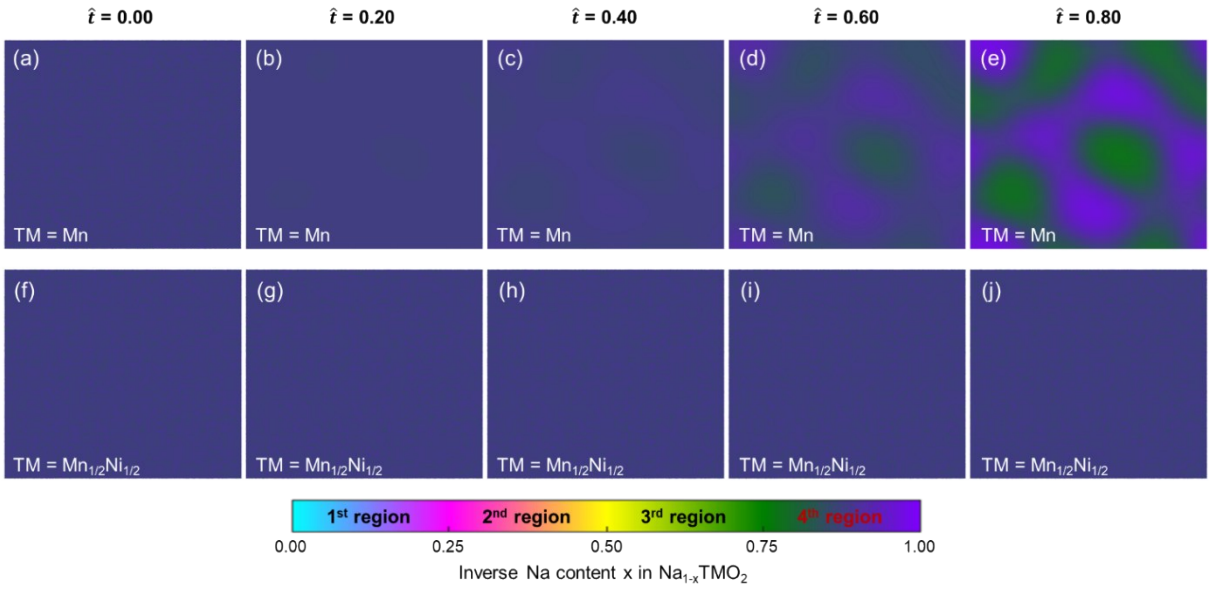

Figure S11. Contours of phase separation kinetics of (a-e) $NaMnO_2$ and (f-j) $Na[Mn_{1/2}Ni_{1/2}]O_2$ in the 4th region at different dimensionless times $\hat{t}$ ($\hat{t}$ = 0.00, 0.20, 0.40, 0.60, and 0.80).

[S1] A.Caballero, L. Hernán, J. Morales, L. Sánchez, J. S. Peña and M. A. G. Aranda, *J. Mater. Chem.*, 2002, **12**, 1142.

[S2] Z. Lu and J. R. Dahn, *J. Electrochem. Soc.*, 2001, **148**, A1225.

[S3] M. Kalapsazova, R. Stoyanova, E. Zhecheva, G. Tyuliev and D. Nihtianova, *J. Mater. Chem. A*, 2014, **12**, 1142.

[S4] Y. Shao, Y.-T. Zhou, M.-M. Deng, Z.-F. Tang, J.-Y. Liao, H. J. M. Bouwmeester and C.-H. Chen, *J. Solid State Electrochem.*, 2019, **23**, 2979.

[S5] D. Kim and J. Lee, *Chem. Mater.*, 2020, **32**, 5541.